Study of the Conformational Transition of Aβ(1−42) Using D-Amino Acid Replacement Analogues†

Katharina Janek,‡ Sven Rothemund,‡ Klaus Gast,§ Michael Beyermann,‡ Josef Zipper,‡ Heinz Fabian,§ Michael Bienert,‡ and Eberhard Krause*,‡

Institute of Molecular Pharmacology and Max Delbrück Center of Molecular Medicine, Berlin, Germany

Received August 23, 2000; Revised Manuscript Received January 5, 2001

ABSTRACT: A critical event in Alzheimer's disease is the transition of Aβ peptides from their soluble forms into disease-associated β-sheet-rich conformers. Structural analysis of a complete D-amino acid replacement set of Aβ(1−42) enabled us to localize in the full-length 42-mer peptide the region responsible for the conformational switch into a β-sheet structure. Although NMR spectroscopy of trifluoroethanol-stabilized monomeric Aβ(1−42) delineated two separated helical domains, only the destabilization of helix I, comprising residues 11−24, caused a transition to a β-sheet structure. This conformational α-to-β switch was directly accompanied by an aggregation process leading to the formation of amyloid fibrils.

The conversion of soluble proteins into fibrillar aggregates is an important event in a considerable number of diseases, including Alzheimer's disease (AD) and prion-related diseases (*1*). All are characterized by a change in protein structure resulting in predominantly β-sheet conformers, which self-associate into insoluble fibrils (amyloid formation). A central event in AD is the formation of amyloid plaques in the brain. The major components of the plaques are 39−43-mer amyloid β-peptides (Aβ) (*2*), which are formed by enzymatic processing of the amyloid β precursor protein (AβPP) (*3*). It has been established that the 42-residue peptide Aβ(1−42) (DAEFRHDSGY^{10}EVHHQKLVFF^{20}-AEDVGSNKGA^{30}IIGLMVGGVV^{40}IA) plays a key role in promoting the disease (*4*). Soluble Aβ (Aβs) at subnanomolar concentration is a normal constituent of human biological fluids (*5*, *6*). Conformational studies to elucidate the structure of Aβs suffer from the tendency of the peptide to form aggregated β-sheets at micro- to millimolar concentration (*7*). NMR studies of monomeric Aβ(1−40) and Aβ-(1−42) stabilized by trifluoroethanol (TFE)[1] or a membrane mimicking environment have indicated a high degree of α-helical secondary structure (*8*−*10*). An α-to-β structural transition has been proposed as a key step initiating peptide aggregation and fibril formation (*11*, *12*). Studies focusing on the association behavior of Aβ using shortened Aβ peptides have shown that fibril formation can be impaired by amino acid substitutions in the central, hydrophobic region between positions 17 and 21 (*13*−*15*). Residues 16−20 are suggested to serve as a binding domain during Aβ aggregation (*16*) and have been targeted in studies aimed at inhibiting the aggregation process (*17*). That hydrophobicity is not the exclusive basis for amyloid formation is underlined by the two single-point mutations linked with early onset amyloidosis: the Flemish (Ala21→Gly) (*18*) and Dutch (Glu22→Gln) (*19*) variants of Aβ.

To assess the impact of conformational alterations on the initiation of amyloid formation, we have studied the influence of D-amino acid substitutions on the secondary structure and association behavior of Aβ(1−42). The replacement of amino acids by their D-enantiomers is known to induce a local destabilization of secondary structures without changing other properties of the peptide (*20*, *21*), thus allowing the separation of conformational from hydrophobic effects. Herein, a complete D-amino acid replacement set was used to locate the region of Aβ(1−42) which modulates the molecular switch into an associating β-sheet structure.

MATERIALS AND METHODS

Peptide Synthesis. Amyloid peptides, Aβ(1−42) and the D-amino acid variants, were synthesized by solid-phase methods on an automated MilliGen 9050 peptide synthesizer (Milligen/Biosearch, Burlington, MA) using Fmoc (N^{α}-9-fluorenylmethoxycarbonyl) chemistry in the continuous flow mode: TentaGel S Ac resin, 0.2 mmol g^{-1} (Rapp Polymere, Tübingen, Germany), 1 equiv of HBTU (*N*-[(1*H*-benzotriazol-1-yl)(dimethylamino)methylene]-*N*-methylmethanaminium hexafluorophosphate *N*-oxide), 2 equiv of DIEA (diisopropylethylamine), coupling time 20 min, deblocking time with 20% piperidine in dimethylformamide, 10 min. Additionally, in the hydrophobic region of residues Ala42 to Lys28 2% DBU (1,8-diazabicyclo[5.4.0]undec-7-ene[1,5-5]) was added during the deblocking step. Peptides were cleaved from the resin support by a mixture of 5% water/5% phenol/2% triisopropylsilane in trifluoroacetic acid for 3 h. The crude peptides were purified by preparative reversed-phase chromatography on PolyEncap A300 (10 μm, 250 × 20 mm i.d., Bischoff Analysentechnik GmbH, Leonberg, Germany), using an acetonitrile/water/0.1% trifluoroacetic acid solvent

† This work was supported by Deutsche Forschungsgemeinschaft Kr 1451/2-2.

* To whom correspondence to should be addressed. Tel: +49-30-94793221. Fax: +49-30-94793159. E-mail: ekrause@fmp-berlin.de.

‡ Institute of Molecular Pharmacology, Robert Rössle Strasse 10, 13125 Berlin, Germany.

§ Max Delbrück Center of Molecular Medicine, Robert Rössle Strasse 10, 13092 Berlin, Germany.

[1] Abbreviations: TFE, trifluoroethanol; CD, circular dichroism; TOCSY, total correlation spectroscopy; NOESY, nuclear Overhauser effect; COSY, correlated spectroscopy; FTIR, Fourier transform infrared; ThT, thioflavin T.

10.1021/bi002005e CCC: $20.00
Published on Web 04/11/2001

system at elevated temperature (85 °C). The separated fractions were evaporated in a vacuum, and the peptides were isolated by lyophilization and analyzed by MALDI mass spectrometry (Voyager-DE STR, Perseptive Biosystems, Framingham, MA) using a sinapinic acid matrix, which gave the expected $[M + H]^+$ mass peaks for each peptide. The peptide content of lyophilized samples was determined by quantitative amino acid analysis (LC 3000 analyzer, Biotronik-Eppendorf, Maintal, Germany). Because trifluoroacetate gives rise to a strong band at ~1673 cm^{-1} in the infrared spectrum which overlaps the conformation-sensitive amide I band of the peptide backbone, all such counterions were replaced by chloride ions by lyophilization twice from 10 mM hydrochloric acid. To ensure that all peptides adopt monomeric, mostly random starting structure stock solutions were prepared by dissolving the lyophilized peptides in pure TFE.

Circular Dichroism Measurements. Circular dichroism (CD) spectra were measured at 25 °C on a J-720 spectropolarimeter (Jasco, Tokyo, Japan), in a quartz cell of 0.1 cm path length, over the range 190−260 nm. The instrument was calibrated with an aqueous solution of (+)-10-camphorsulfonic acid. CD spectra were the average of a series of six scans made at 0.1 nm intervals. Peptide concentrations were 2×10^{-5} M in 80% TFE/20% H_2O (v/v). The CD results are reported as mean residue molar ellipticity [Θ] in deg cm^2/dmol. The amount of helix was estimated from the relation: helicity (%) = $([\Theta]_{222} - [\Theta]^0_{222})/[\Theta]^{100}_{222}$, where $[\Theta]_{222}$ is the determined mean residue ellipticity at 222 nm. For $[\Theta]^0_{222}$ and $[\Theta]^{100}_{222}$, representing 0 and 100% helix content, values of −2340 and −30300 deg cm^2/dmol, respectively, were used (*22*).

NMR Spectroscopy and Structure Calculations. Aβ(1−42) was dissolved in 80% TFE-d_2-OH/20% water (v/v) to a final concentration of 2 mM. The pH was adjusted to 2.5. The ^{1}H NMR spectra were acquired on a standard Bruker DMX 600 spectrometer at 300 K. Typical acquisition parameters were a spectral width of 8333 Hz and a pulse width (90 °) of 10.1 μs. One-dimensional spectra did not change over the concentration range 0.5−2.0 mM, suggesting that the peptide was monomeric under the experimental conditions. For two-dimensional spectra 4 K complex data points, 32 transients, and 512 complex increments were collected. Double-quantum-filtered phase-sensitive 2D correlated spectroscopy (DQF-COSY) (*23*) and 2D total correlation spectroscopy (TOCSY) (*24*, *25*) were used for spin-type assignments. Sequential assignments were made using phase-sensitive 2D nuclear Overhauser effect spectroscopy (NOESY) (*26*) and standard procedures (*27*). Several mixing times between 100 and 200 ms for NOESY and 60−85 ms for TOCSY spectra were acquired. The data sets were processed using shifted sine-bell apodization and zero filling in both dimensions. Spectra were processed under Linux using the NMRPipe software system (*28*) and analyzed with the program NMRview (*29*). Peak intensities were estimated from NOESY spectra. The peaks were divided into three categories and assigned distance ranges according to their intensity: strong, 1.5−3.0 Å; medium, 1.5−3.3 Å; and weak, 1.5−5.0 Å. Overlapped cross-peaks were given a value of 1.5−5.0 Å. Pseudoatom correction was used to adjust distances involving nonstereospecifically assigned protons such as methyl, methylene, or aromatic ring protons. Distance geometry and molecular dynamic (MD) calculations were performed with the X-PLOR 3.1 package (*30*) employing the hybrid distance geometry-restrained MD approach with simulated annealing refinement and subsequent energy minimization (standard protocols) (*30*). The calculation started from an extended template including the experimental data of 107 intraresidual and 157 interresidual NOE distance restraints. No long-range NOE cross-peaks were observed. Out of 50 resulting structures, 15 final structures (with no distance restraint violations greater than 0.03 Å or dihedral angle restraint violations in excess of 1°) were included in an ensemble for further characterization. For visualization of structure data the MOLMOL package (*31*) was used.

Fourier Transform Infrared Spectroscopy. Infrared spectra were collected on an IFS-66 FTIR (Bruker, Karlsruhe, Germany) spectrometer equipped with a DT65 detector with continuous purging by dry air. Measurements were performed in 80% TFE-d_3/20% deuterium oxide (v/v). All data were obtained from freshly prepared solutions at a peptide concentration of 4.4×10^{-4} M. The samples were placed between a pair of CaF_2 windows, separated by a path length of 50 μm. The solvent spectrum was recorded under identical conditions and subtracted from the peptide spectra. For each sample, 128 interferrograms were coadded and Fourier transformed to generate a spectrum with a nominal resolution of 4 cm^{-1}. Residual water vapor was interactively subtracted, as described previously (*32*). The final unsmoothed peptide spectra were used for further analysis. Band narrowing of the spectra by Fourier self-deconvolution, which leads to a better visualization of overlapping bands, was carried out using a half-bandwidth of 16 cm^{-1} and a band narrowing factor, $k = 1.6$.

Dynamic Light Scattering. Dynamic light scattering (DLS) measurements were performed at a scattering angle of 90° with a laboratory-built setup (*33*), equipped with an argon laser Lexel 3500 (Lexel Inc., CA) operating at 514.5 nm wavelength and 0.5 W output power. The peptide solutions (1 mg mL^{-1} in 80% TFE/20% water, v/v) were filtered through 100 nm pore-size Anodisc filters (Whatman, U.K.) into 50 μL flow-through cells, which fit the cell holders of both the DLS setup and a Beckman DU-650 spectrophotometer. Peptide concentrations before and after filtration were determined spectrophotometrically using a calculated absorbance (*34*) A(276 nm, 1 cm, 1 mg mL^{-1}) = 0.32. The temperature during measurement was 20 °C. The scattered light intensity was measured with the same setup using benzene as a reference sample. Distribution functions of translational diffusion coefficients D and the corresponding size distributions in terms of the hydrodynamic Stokes radius were obtained from the measured autocorrelation functions with the program CONTIN (*35*). The size distributions consisted of two major peaks indicating that the peptides were present as both monomers and aggregates. The distribution functions were normalized such that the peak areas a_M and a_A are proportional to the fractions of the total light scattering intensity of monomers or aggregates, respectively. The extent of aggregation can be estimated from the ratio a_A/a_M only if the shape of aggregates is approximately known, since the scattering intensity depends on the weight concentration, the mass, and the scattering function of the particles. Estimates have been made for Aβ(1−42) and D-21/22 by following a number of assumptions. According to the

electron microscopic results, the aggregates were modeled by cylinders with a diameter of 8 nm and an average length, calculated from the Stokes radius according to the cylindrical shell model (*36*). The average mass was obtained using a mass per length ratio of 7 kDa/nm (*37*). The scattering function of rigid rods was applied. For the small monomers with a mass of 4.5 kDa the scattering function is 1.

Thioflavin T Fluorescence Assay. For Thioflavin T (ThT) analysis, which was described previously (*38*), 40 μL of the peptide solution (1 mg mL^{-1} in 80% TFE/20% water, v/v) was added to 3 μM ThT in 50 mM glycine, pH 9.1, in a final volume of 2 mL. Immediately thereafter, the fluorescence was monitored at E_{ex} = 450 nm and E_{em} = 482 nm on a Perkin-Elmer LS 50B spectrofluorometer at 25 °C. A time scan was performed. The value after 240 s, when a plateau was reached, was subtracted from the background signal of the 3 μM ThT solution. All experiments were carried out in duplicate.

Electron Microscopy. The analogue D-21/22 was dissolved in 80% TFE/20% water (v/v) at a concentration of 1 mg mL^{-1}. A 5 μL aliquot was adsorbed for 60 s onto 300-mesh copper grids coated with carbon film (support films made from Formavar or Pioloform were destroyed by TFE). Excess liquid was removed with filter paper. The air-dried sample on the grid was negatively stained with 5 μL of freshly prepared 2% (w/v) uranyl acetate in water. After 60 s the excess liquid was removed, and the sample was allowed to air-dry. Specimens were examined with a 902 A electron microscope (Zeiss, Oberkochen, Germany) at 80 kV.

RESULTS AND DISCUSSION

The structural analysis of the double D-amino acid replacement set of Aβ(1−42) was performed in the presence of the α-helix-inducing solvent TFE to maintain a monomeric, soluble peptide conformation. CD measurements at different TFE concentrations have shown that Aβ(1−42) adopts a structure with a helix fraction between 0.40 and 0.45 in 80% TFE/20% water. Lower concentrations of TFE resulted in destabilization of the α-helical conformation and subsequent increase of β-sheet structure. NMR spectroscopy to localize secondary structure elements was carried out in 80% TFE, even though NMR studies were previously performed in 40% TFE for Aβ(1−40) (*8*) and in micellar sodium dodecyl sulfate (SDS) solution for Aβ(1−40) and Aβ(1−42) (*9*, *10*). Figure 1 shows NH(*i*) to NH(*i*+1) connectivities and Table 1 shows the chemical shifts of the proton resonances of Aβ-(1−42). Numerous medium-range CαH(*i*)−NH(*i*,*i*+3) and CαH(*i*)−CβH(*i*,*i*+3) NOE connectivities were observed for the regions Glu11−Val24 and Lys28−Val36, suggesting the existence of two α-helical domains in Aβ(1−42). This result was supported by analysis of α-proton chemical shift deviations from "random coil" reference values (*39*) (data not shown). A set of 287 conformational restraints derived from NMR analysis was used for distance geometry calculations. Statistical data are shown in Table 2. The most prominent features in the structure of Aβ(1−42) include two well-defined α-helices in the segments Glu11−Val24 and Lys28−Val36, shown as best-fit superpositions in Figure 2. From the lack of NOE restraints the linker connecting the two helices would appears to be quite flexible. Overall, the results obtained in the presence of 80% TFE agree well with NMR studies suggesting two stable and well-defined α-helices, comprising Gln15−Asp23 and Ile31−Met35 in the presence of 40% TFE (*8*) and Gln15−Val24 and Lys28−

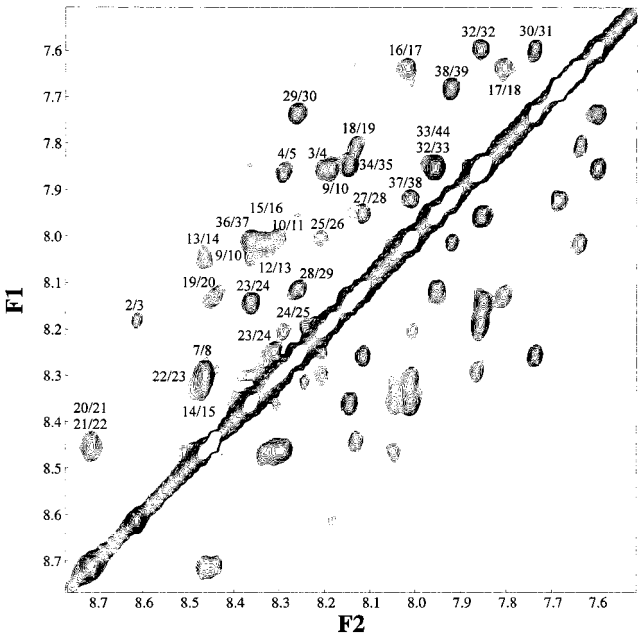

FIGURE 1: Two-dimensional NMR spectroscopy of unmodified Aβ-(1−42) in 80% TFE/20% water. NH(*i*) to NH(*i*+1) connectivities of a 600 MHz NOESY ^{1}H NMR spectrum.

Table 1: Spin System Assignments for Unmodified Aβ(1−42) in 80% TFE/20% Water

	chemical shifts (ppm)							
AA[a]	NH	CαH	Cβ H		Cγ H		others	
D1		4.248	2.985	3.082				
A2	8.560	4.244	1.375					
E3	8.134	4.128	2.031	2.070	2.403[b]			
F4	7.805	4.428	3.103	3.191	7.190	7.150		
R5	8.241	4.046	1.798	1.921	1.589	1.620	3.151	7.150
H6	8.238	4.527	3.248	3.322			7.255	
D7	8.414	4.673	2.910[b]					
S8	8.246	4.257						
G9	8.310	3.998[b]						
Y10	7.954	4.248	3.114	3.114			6.714	7.047
E11	8.259	4.079	2.292[b]		2.572[b]			
V12	8.313	3.742	2.105		1.056	0.898		
H13	7.998	4.234	3.265[b]				7.246	
H14	8.416	4.203	3.280[b]				7.166	
Q15	8.286	3.907	2.139	2.227	2.335[b]		6.263	6.539
K16	7.968	4.060	1.951		1.470		1.659	2.902
L17	7.590	4.206	1.717	1.472	1.695		0.842	
V18	7.755	3.595	2.024		0.832[b]			
F19	8.084	4.335	3.213[b]				7.165	7.246
F20	8.405	4.248	3.300[b]					
A21	8.661	3.930	1.533					
E22	8.410	4.089	2.075	2.190	2.407	2.632		
D23	8.257	4.454	2.776	2.776				
V24	8.204	3.694	1.870		0.698	0.795		
G25	8.156	3.836	3.865					
S26	7.958	4.353	3.990[b]					
N27	7.906	4.723	2.832	2.905			6.431	7.289
K28	8.068	4.131	1.867	1.908	1.468	1.529	1.670	2.970
G29	8.209	3.839[b]						
A30	7.687	4.210	1.468					
I31	7.551	3.928	1.983		1.259	0.955	0.875	
I32	7.802	4.214	1.910		1.237	0.910	0.865	
G33	7.906	3.842	3.808					
L34	7.805	4.225	1.610[b]				0.863[b]	
M35	8.096	4.320	2.137	2.271	2.532	2.713		
V36	8.312	4.000	2.197		0.944	1.014		
G37	7.961	3.873	3.931					
G38	7.870	3.936[b]						
V39	7.635	4.061	2.123		0.908	0.944		
V40	7.600	4.068	2.059		0.906	0.938		
I41	7.630	4.341	1.398		0.958[b]			
A42	8.442	4.254	1.339					

[a] Amino acid. [b] Degenerated shifts.

Table 2: Structure Statistics for 15 Best Structures of Aβ(1−42) after Energy Minimization and Simulated Annealing

restraints for structure calculations	
total restraints	287
total NOE restraints	264
intraresidue	107
sequential	80
medium range	77
J-coupling restraints	23
statistics for structure calculations	
rmsd from idealized geometry	⟨*SA*⟩
bonds (Å)	0.0019 ± 0.0001
bond angles (deg)	0.489 ± 0.007
improper torsions (deg)	0.415 ± 0.011
NOEs	0.028 ± 0.001
J-coupling constraints	0.010 ± 0.001
final energies (kcal mol^{-1})	
E_{total}	66.88 ± 1.97
E_{bonds}	2.20 ± 0.19
E_{angles}	40.87 ± 1.28
$E_{improper}$	8.56 ± 0.44
E_{vdW}	3.79 ± 0.46
E_{NOE}	10.70 ± 0.70
$E_{J-coupling}$	0.70 ± 0.20
coordinate precision (Å)	⟨*SA*⟩ vs ⟨SA_{av}⟩
rmsd of backbone atoms (N, Cα, C′)	
for residues 11−24	0.64 ± 0.21
for residues 28−36	0.57 ± 0.17
rmsd of all heavy atoms	
for residues 11−24	1.19 ± 0.21
for residues 28−36	0.95 ± 0.17
PROCHECK Ramachandran plot statistics	
residues in most favored regions	60.8
residues in additional allowed regions	32.0
residues in generously allowed regions	4.0
residues in disallowed regions	3.1

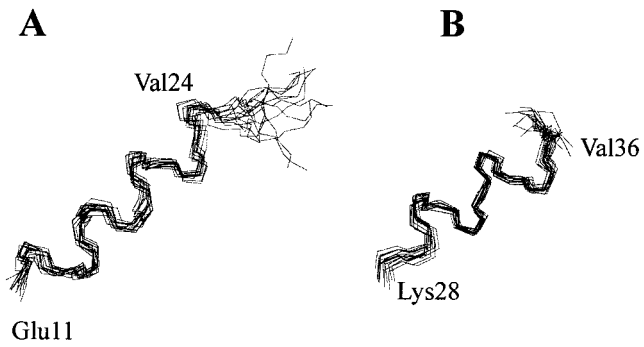

FIGURE 2: Structural calculations of Aβ(1−42). Best-fit backbone superpositions of NMR structures of the two helical regions (A) Glu11−Val24 and (B) Lys28−Val36 of Aβ(1−42). For clarity, 15 structures out of 50 were chosen.

Val36 in micellar SDS solution (*9*, *10*). The observed deviations in helix lengths may be due to the differing contents of the structure-stabilizing solvent TFE (40% versus 80%) and the effect of structure induction/stabilization during the interaction with SDS micelles.

To destabilize the α-helical conformation of Aβ(1−42) position-specifically, a double D-amino acid replacement set was synthesized (Table 3). Although it had been reported that synthesis of the full-length Aβ was problematical (*40*, *41*), we were able to synthesize the native sequence and 20 variants without problems using Fmoc chemistry and standard protocols. The set consists of peptides with a pairwise replacement of adjacent amino acids by their D-enantiomers. Double rather than single substitutions were performed to enhance the effect of secondary structure disturbance (*20*). The replacement of amino acids by their D-enantiomers induces a local destabilization of α-helical structures without changing other peptide properties, such as hydrophobicity, side chain functionality, or charge distribution (*20*, *21*). Complete replacement sets have been previously used to localize helical domains in neuropeptides (*20*, *42*), as well as to study the role of peptide helicity on the interaction of antibacterial peptides with lipid bilayers and biological membranes (*43*). Changes in secondary structure induced by D-amino acid substitution were studied by CD and Fourier transform infrared (FTIR) spectroscopy. CD measurements (Figure 3) indicated a position-dependent destabilization of the α-helical Aβ(1−42). While most of the analogues remained α-helical (e.g., peptide D-5/6), there was a strong reduction of helicity by substitution in the central region (residues 17−21). The CD spectra of these analogues indicated a transition to a β-structure. FTIR is particularly well suited for independent detection of α-helical and β-sheet structures. The results of our FTIR experiments, which are consistent with the CD data, also indicate an α-to-β transition of Aβ(1−42) after directed D-amino acid replacement. The spectra of Aβ(1−42) and most D-analogues are characterized by an amide I band at 1654 cm^{-1}, which can be assigned to an α-helical structure (Figure 4A). However, the IR spectra of some D-analogues (within helix I) reveal an additional feature: a band at 1634 cm^{-1}, which is typical of β-sheet structures. Plotting of the quotient of β- and α-amide I bands as a function of the D-amino acid replacement (Figure 4B) clearly indicates the destabilization of helix I (11−24) by substitution of residues 17−24 (LVFFAEDV), and to a lesser degree of residues 10−12 (YEV), leading to an α-to-β transition in the peptide. The weak influence of the substitutions of residues 13−16 (HHQK) on the conformational switch could be explained by the different helix-destabilizing propensities of D-amino acids. Compared to a substitution of Val/Val by D-Val/D-Val in a helical host model peptide, the destabilizing effect of His/His by D-His/D-His is dramatically weaker, as recently shown by measurements of changes in free energy of 7.1 and 1.6 kJ/mol, respectively (*44*). Both CD and FTIR experiments revealed that the potential to cause an α-to-β transition of Aβ(1−42) is located within helix I (residues 11−24). In contrast, D-amino acid substitution in neither helix II (28−36) nor the N- or C-terminus caused such a conformational transition. That helix I should indeed be responsible for the α-to-β-switch was underlined by studies with shortened Aβ peptides. While the C-terminal fragment, Aβ(29−42), is β-structured regardless of pH or temperature, the N-terminal peptide Aβ(1−28) can adopt different conformations depending on the enviroment (*7*, *45*). The strongest effect on helix destabilization of Aβ(1−42) and therefore on the conformational switch into a β-sheet structure was produced by D-amino acid substitution within residues 19−22. This is exactly the region where the point mutations Ala21→Gly of the Flemish and Glu22→Gln of the Dutch type of Aβ are located. That these mutations destabilize the secondary structure has been shown by previous studies. It was demonstrated by using fragment Aβ-(19−35) that the substitution Ala21→Gly alters the secondary structure in TFE from α-helix toward β-sheet (*46*). The Dutch mutation decreases the propensity of the central region of Aβ to adopt an α-helical conformation according to the Chou−Fasman method (*47*). This was shown to result in a conformer with a higher β-sheet content (*48*). In contrast, α-helix stabilization by the single mutation Val18→Ala in Aβ(1−40) results in a less amyloidogenic peptide analogue (*11*). The importance of the Aβ domain 11−24 is underlined

Table 3: Aβ(1−42) Double D-Amino Acid Replacement Set

Peptide	Sequence[a]	D-Amino Acid Substitution
Aβ(1−42)	DAEFRHDSGY[10]EVHHQKLVFF[20]AEDVGSNKGA[30]IIGLMVGGVV[40]IA	-
D-1/2	**DA**EFRHDSGY[10]EVHHQKLVFF[20]AEDVGSNKGA[30]IIGLMVGGVV[40]IA	**d1/a2**
D-3/4	DA**EF**RHDSGY[10]EVHHQKLVFF[20]AEDVGSNKGA[30]IIGLMVGGVV[40]IA	**e3/f4**
D-5/6	DAEF**RH**DSGY[10]EVHHQKLVFF[20]AEDVGSNKGA[30]IIGLMVGGVV[40]IA	**r5/h6**
D-7/8	DAEFRH**DS**GY[10]EVHHQKLVFF[20]AEDVGSNKGA[30]IIGLMVGGVV[40]IA	**d7/s8**
D-10/11	DAEFRHDSG**Y**[10]**E**VHHQKLVFF[20]AEDVGSNKGA[30]IIGLMVGGVV[40]IA	**y10/e11**
D-11/12	DAEFRHDSGY[10]**EV**HHQKLVFF[20]AEDVGSNKGA[30]IIGLMVGGVV[40]IA	**e11/v12**
D-13/14	DAEFRHDSGY[10]EV**HH**QKLVFF[20]AEDVGSNKGA[30]IIGLMVGGVV[40]IA	**h13/h14**
D-15/16	DAEFRHDSGY[10]EVHH**QK**LVFF[20]AEDVGSNKGA[30]IIGLMVGGVV[40]IA	**q15/k16**
D-17/18	DAEFRHDSGY[10]EVHHQK**LV**FF[20]AEDVGSNKGA[30]IIGLMVGGVV[40]IA	**l17/v18**
D-19/20	DAEFRHDSGY[10]EVHHQKLV**FF**[20]AEDVGSNKGA[30]IIGLMVGGVV[40]IA	**f19/f20**
D-21/22	DAEFRHDSGY[10]EVHHQKLVFF[20]**AE**DVGSNKGA[30]IIGLMVGGVV[40]IA	**a21/e22**
D-23/24	DAEFRHDSGY[10]EVHHQKLVFF[20]AE**DV**GSNKGA[30]IIGLMVGGVV[40]IA	**d23/v24**
D-26/27	DAEFRHDSGY[10]EVHHQKLVFF[20]AEDVG**SN**KGA[30]IIGLMVGGVV[40]IA	**s26/n27**
D-27/28	DAEFRHDSGY[10]EVHHQKLVFF[20]AEDVGS**NK**GA[30]IIGLMVGGVV[40]IA	**n27/k28**
D-30/31	DAEFRHDSGY[10]EVHHQKLVFF[20]AEDVGSNKG**A**[30]**I**IGLMVGGVV[40]IA	**a30/i31**
D-31/32	DAEFRHDSGY[10]EVHHQKLVFF[20]AEDVGSNKGA[30]**II**GLMVGGVV[40]IA	**i31/i32**
D-34/35	DAEFRHDDGY[10]EVHHQKLVFF[20]AEDVGSNKGA[30]IIG**LM**VGGVV[40]IA	**l34/m35**
D-35/36	DAEFRHDDGY[10]EVHHQKLVFF[20]AEDVGSNKGA[30]IIGL**MV**GGVV[40]IA	**m35/v36**
D-39/40	DAEFRHDDGY[10]EVHHQKLVFF[20]AEDVGSNKGA[30]IIGLMVGG**VV**[40]IA	**v39/v40**
D-41/42	DAEFRHDDGY[10]EVHHQKLVFF[20]AEDVGSNKGA[30]IIGLMVGGVV[40]**IA**	**i41/a42**

[a] D-Amino acids are underlined.

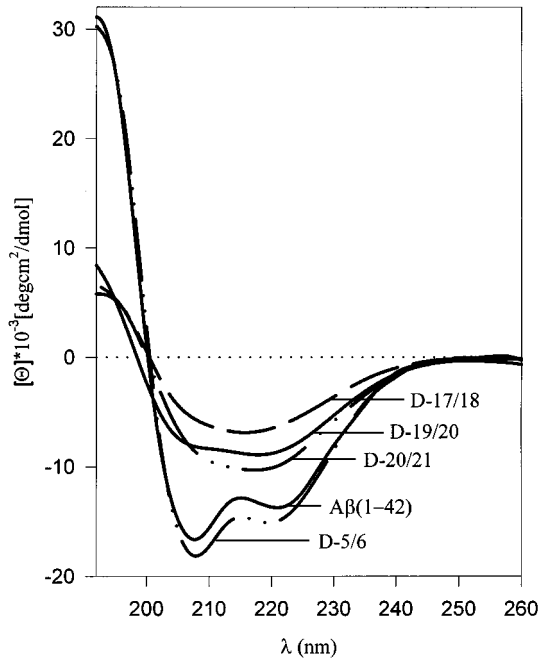

FIGURE 3: Effect of D-amino acid substitutions on the helix stability of Aβ(1−42). CD studies were performed in 80% TFE/20% water at a peptide concentration of 2×10^{-5} M.

by the interaction of the peptide with molecules such as apolipoprotein E (ApoE), glycosaminoglycans, or nicotine, which influence amyloid formation. ApoE and glycosaminoglycans were found to interact with amino acids 12−28 and 12−17 of Aβ, respectively (*49*, *50*). Both promote the formation of amyloid fibrils. The inhibitory effect of nicotine on amyloid formation of Aβ(1−42) is thought to involve its binding to the α-helical domain within residues 1−28, thereby preventing an α-to-β conformational transition (*51*).

To investigate whether the α-to-β transition observed is linked to an association process which leads to amyloid fibrils, static and dynamic light scattering experiments, the ThT fluorescence assay, and electron microscopic experiments were performed. Combined static and dynamic light scattering allowed determination of the relative scattered intensity I_{rel} and the distribution function of Stokes radii R_S, which can be used to estimate the degree of association. Because filtration of the sample is indispensable for light scattering experiments, the removal of a significant amount of aggregate had to be taken into consideration. Therefore, the amount of separated high molecular weight aggregates was quantified (Table 4). Remarkably, about 50% of the peptide was retained in the case of D-19/20 and D-21/22, indicating that strong association processes are initiated by the α-to-β transition. The analogue D-17/18 was also found to undergo association into high molecular peptide assemblies although to a much lesser extent. In comparison, no high molecular weight aggregates were observed for the α-helical Aβ(1−42) itself. The different association behaviors of these peptides were also reflected by the results of subsequent light scattering investigations of the filtrates, particularly by the relative scattered intensities I_{rel} (Table 4). Compared to that of the nonmodified Aβ(1−42) molecule, the intensities were significantly increased for analogues with substitution in positions 19−24, which indicates significant aggregation. Interestingly, analogue D-11/12, which has also been shown to undergo an α-to-β transition, did not exhibit any increased association behavior. The DLS size distributions always displayed two major peaks, one with $R_S = 1.1 \pm 0.1$ nm, derived of peptide monomers, and the second ($R_{S,A}$ in Table 4) representing the average hydrodynamic radius of the peptide aggregates present. The corresponding peak area, a_A, in the size distribution function varied considerably in concert with the relative scattered intensities I_{rel}. An estimation of the amount of aggregates in the filtrate, which was performed for both Aβ(1−42) as the wild-type sequence and the modified analogue D-21/22 (see Materials and Methods),

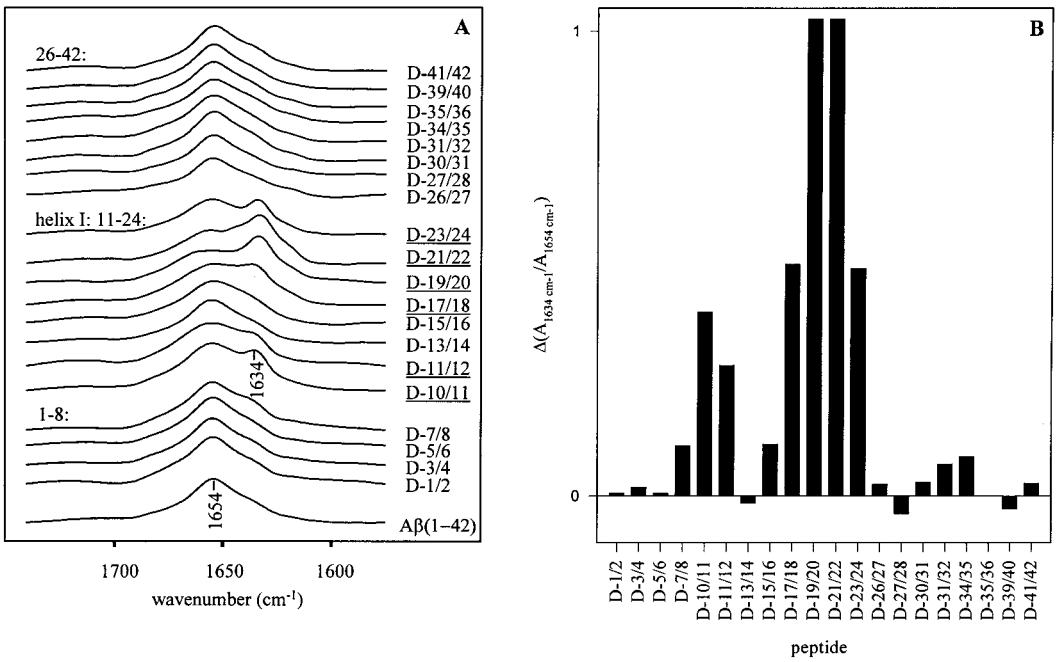

FIGURE 4: Conformational α-to-β transition of Aβ(1−42) induced by position-specific D-amino acid replacement. (A) FTIR spectra in the amide I region of the complete Aβ(1−42) D-amino acid replacement set recorded in 80% TFE-d_3/20% deuterium oxide at a peptide concentration of 5×10^{-4} M. (B) Quotient of intensities of the β-band and α-band ($A_{1634cm^{-1}}/A_{1654cm^{-1}}$) of D-amino acid substituted peptides relative to Aβ(1−42).

Table 4: Association Behavior of Aβ(1−42) and Selected D-Analogues in 80% TFE

	filtration step[a]	dynamic light scattering of the filtered peptide sample	
peptide	amount of aggregates retained (%)	I_{rel}	$R_{S,A}$ (nm)
Aβ(1−42)	0	0.4	21
D-1/2	5	3.0	22
D-11/12	0	0.8	14
D-17/18	12	2.8	17
D-19/20	44	12.1	29
D-21/22	53	12.1	24
D-23/24	3	6.3	19
D-34/35	0	4.4	20

[a] 100 nm pore size filter.

suggests no aggregation in the former case but 30% in the latter. The ThT fluorometric assay was performed to test whether the aggregates formed are fibrillar in character. ThT interacts specifically with amyloid fibrils, thereby undergoing a shift in its excitation and emission maximum (*38*). The analogue D-21/22, which had shown the strongest association behavior, was selected and compared to Aβ(1−42). As expected, there was no interaction of ThT with the α-helical Aβ(1−42) in TFE (1.8 fluorescence units). In contrast, peptide D-21/22 showed a strong binding to ThT (747 fluorescence units), indicating that the aggregates formed are of fibrillar morphology. The fibrillar structure of the aggregates was confirmed by electron microscopy (Figure 5). Unbranched fibrils, on average 8 nm wide and 100 nm to >1 μm long, were observed, corresponding in appearance and dimensions to ordinary amyloid fibrils (*52*).

Taken together, the results of the association experiments in TFE show that destabilization of helix I (11−24) between positions 17 and 24 is accompanied by association into amyloid fibrils. The strongest association was found for the analogues D-19/20 and D-21/22. In contrast, neither D-amino

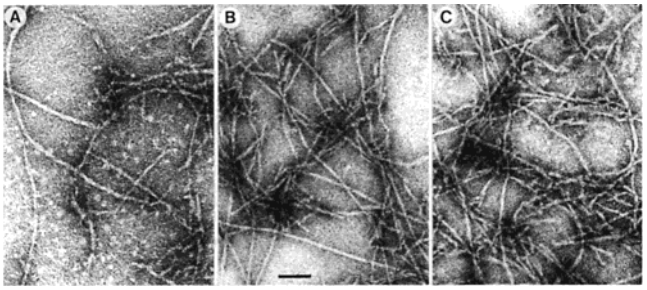

FIGURE 5: Fibril formation of D-21/22. Electron micrographs of negatively stained (2% uranyl acetate) fibrils of the D-amino acid substituted analogue D-21/22 (1 mg mL^{-1}) in 80% TFE/20% water. Bar: 100 nm.

acid substitution in positions 10−12, also shown to cause a conformational transition of the peptide, but to a lesser degree than substitutions in the region 17−24, nor replacement in all other positions was found to lead to such strong increases in association. These facts correspond to the finding that the isomerization of aspartyl residues within the central region (isoAsp23) strongly increases Aβ(1−42) aggregation, while the influence of isomerization at position 7 is rather weak (*41*). The finding that structure disruption in the region between residues 17 and 24 of Aβ(1−42) initiates an α-to-β transition which is accompanied by amyloid formation provides evidence that this domain not only has a key role in the association process because of hydrophobic interactions (*13*) but directly causes a switch of secondary structure of the Alzheimer peptide.

CONCLUSIONS

The results of the present study have shown that the conformational switch of Aβ(1−42) into a β-structure could be initiated by destabilization of the α-helical domain comprising residues 11−24. The D-amino acid induced α-to-β transition is accompanied by association into amyloid

fibrils. Most important for the conformational switch, and therefore for amyloid formation, are residues 17−24, which are located in the hydrophobic region of the helix. This region has been suggested to serve as a binding domain during Aβ aggregation (*16*, *17*). Thus both the conformational shift and the hydrophobicity of the central helix are important driving forces in this process.

ACKNOWLEDGMENT

We thank Joachim Behlke for helpful discussions concerning the association measurements, Dagmar Smettan and Anne Klose for technical assistance, and Louis A. Carpino and John Dickson for critical reading of the manuscript.

REFERENCES

1. Carrell, R. W., and Lomas, D. A. (1997) *Lancet 350*, 134−138.
2. Glenner, G. G., and Wong, C. W. (1984) *Biochem. Biophys. Res. Commun. 120*, 885−890.
3. Kang, J., Lemaire, H. G., Unterbeck, A., Salbaum, J. H., Masters, C. L., Grzeschik, K. H., Multhaupt, G., Beyreuther, K., and Muller-Hill, B. (1987) *Nature 325*, 733−736.
4. Hardy, J. (1997) *Trends Neurosci. 20*, 154−159.
5. Seubert, P., Vigo-Pelfrey, C., Esch, F., Lee, M., Dovey, H., Davis, D., Siha, S., Schlossmacher, M., Whaley, J., Swindlehurst, C., McCormack, R., Wolfert, R., Selkoe, D., Lieberburg, I., and Schenk, D. (1992) *Nature 359*, 325−327.
6. Shoji, M., Golde, T. E., Ghiso, J., Cheung, T., Estus, S., Shaffer, L. M., Cai, X. D., McKay, D. M., Tintner, R., Frangione, B., and Younkin, S. G. (1992) *Science 258*, 126−129.
7. Barrow, C. J., Yasuda, A., Kenny, P. T., and Zagorski, M. G. (1992) *J. Mol. Biol. 225*, 1075−1093.
8. Sticht, H., Bayer, P., Willbold, D., Dames, S., Hilbich, C., Beyreuther, K., Frank, R. W., and Rosch, P. (1995) *Eur. J. Biochem. 233*, 293−298.
9. Coles, M., Bicknell, W., Watson, A. A., Fairlie, D. P., and Craik, D. J. (1998) *Biochemistry 37*, 11064−11077.
10. Shao, H., Jao, S., Ma, K., and Zagorski, M. G. (1999) *J. Mol. Biol. 285*, 755−773.
11. Soto, C., Castano, E. M., Frangione, B., and Inestrosa, N. C. (1995) *J. Biol. Chem. 270*, 3063−3067.
12. Mihara, H., Takahashi, Y., and Ueno, A. (1998) *Biopolymers 47*, 83−92.
13. Hilbich, C., Kisters-Woike, B., Reed, J., Masters, C. L., and Beyreuther, K. (1992) *J. Mol. Biol. 228*, 460−473.
14. Wood, S. J., Wetzel, R., Martin, J. D., and Hurle, M. R. (1995) *Biochemistry 34*, 724−730.
15. Esler, W. P., Stimson, E. R., Ghilardi, J. R., Lu, Y. A., Felix, A. M., Vinters, H. V., Mantyh, P. W., Lee, J. P., and Maggio, J. E. (1996) *Biochemistry 35*, 13914−13921.
16. Tjernberg, L. O., Naslund, J., Lindqvist, F., Johansson, J., Karlstrom, A. R., Thyberg, J., Terenius, L., and Nordstedt, C. (1996) *J. Biol. Chem. 271*, 8545−8548.
17. Soto, C., Sigurdsson, E. M., Morelli, L., Kumar, R. A., Castano, E. M., and Frangione, B. (1998) *Nat. Med. 4*, 822−826.
18. Hendriks, L., Van Duijn, C. M., Cras, P., Cruts, M., van Hul, W., van Harskamp, F., Warren, A., McInnis, M. G., Antonarakis, S. E., Martin, J. J., Hofman, A., and van Broeckhoven (1992) *Nat. Genet. 1*, 218−221.
19. Levy, E., Carman, M. D., Fernandez-Madrid, I. J., Power, M. D., Lieberburg, I., van Duinen, S. G., Bots, G. T., Luyendijk, W., and Frangione, B. (1990) *Science 248*, 1124−1126.
20. Krause, E., Beyermann, M., Dathe, M., Rothemund, S., and Bienert, M. (1995) *Anal. Chem. 67*, 252−258.
21. Rothemund, S., Beyermann, M., Krause, E., Krause, G., Bienert, M., Hodges, R. S., Sykes, B. D., and Sonnichsen, F. D. (1995) *Biochemistry 34*, 12954−12962.
22. Chen, Y., Yang, J. T., and Martinez, H. M. (1972) *Biochemistry 11*, 4120−4131.
23. Piantini, U., Sorensen, O. W., and Ernst, R. R. (1982) *J. Am. Chem. Soc. 104*, 6800−6801.
24. Braunschweiler, L., and Ernst, R. R. (1983) *J. Magn. Reson. 53*, 521−528.
25. Davis, D. G., and Bax, A. (1985) *J. Am. Chem. Soc. 107*, 2820−2821.
26. Jeener, J., Meier, B. H., Bachmann, P., and Ernst, R. R. (1979) *J. Chem. Phys. 71*, 4546−4553.
27. Wüthrich, K. (1986) *NMR of proteins and nucleic acids*, Wiley, New York.
28. Delaglio, F., Grzesiek, S., Vuister, G., Zhu, G., Pfeifer, J., and Bax, A. (1995) *J. Biomol. NMR 6*, 277−293.
29. Johnson, B. A., and Blevins, R. A. (1994) *J. Biomol. NMR 4*, 603−614.
30. Brünger, A. T. (1993) *X-PLOR Manual Version 3.1. A system for X-ray crystallography and NMR*, Yale University Press, New Haven, CT.
31. Koradi, R., Billeter, M., and Wüthrich K. (1996) *J. Mol. Graphics 14*, 51−55.
32. Fabian, H., Schultz, C., Naumann, D., Landt, O., Hahn, U., and Saenger, W. (1993) *J. Mol. Biol. 232*, 967−981.
33. Gast, K., Nöppert, A., Müller-Frohne, M., Zirwer, D., and Damaschun, G. (1997) *Eur. Biophys. J. 25*, 211−219.
34. Gill, S. C., and von Hippel, P. H. (1998) *Anal. Biochem. 182*, 319−326.
35. Provencher, S. W. (1982) *Comput. Phys. Commun. 27*, 229−242.
36. De La Torre, G. J., and Bloomfield, V. A. (1981) *Q. Rev. Biophys. 14*, 81−139.
37. Lomakin, A., Chung, D. S., Benedek, G. B., Kirschner, D. A., and Teplow, D. B. (1996) *Proc. Natl. Acad. Sci. U.S.A. 93*, 1125−1129.
38. LeVine, H., III (1993) *Protein Sci. 2*, 404−410.
39. Wishard, D. S., Bigan, C. G., Holm, A., Hodges, R. S., and Syke, B. D. (1995) *J. Biomol. NMR 5*, 67−81.
40. Fukuda, H., Shimizu, T., Nakajima, M., Moro, H., and Shirasawa, T. (1999) *Bioorg. Med. Chem. Lett. 9*, 953−956.
41. Berger, E. P., Rasmussen, K. C., Weinreb, P. H., and Lansbury, P. T., Jr. (1994) *Peptides. Chemistry, Structure and Biology (*Hodges, R. S., and Smith, J. A., Eds.) pp 502−504, Escom, Leiden.
42. Krause, E., Rothemund, S., Beyermann, M., and Bienert, M. (1997) *Anal. Chim. Acta 352*, 365−374.
43. Wieprecht, T., Dathe, M., Schümann, M., Krause, E., Beyermann, M., and Bienert, M. (1996) *Biochemistry 35*, 10844−10853.
44. Krause, E., Bienert, M., Schmieder, P., and Wenschuh, H. (2000) *J. Am. Chem. Soc. 122*, 4865−4870.
45. Barrow, C. J., and Zagorski, M. G. (1991) *Science 253*, 179−182.
46. El-Agnaf, O. M. A., Guthrie, D. J., Walsh, D. M., and Irvine, G. B.(1998) *Eur. J. Biochem. 256*, 560−569.
47. Chou, P. Y., and Fasman, G. D. (1978) *Adv. Enzymol. Relat. Areas Mol. Biol. 47*, 45−148.
48. Fabian, H., Choo, L.-P., Szendrei, G. I., Jackson, M., Halliday, W. C., Otvos, L., and Mantsch, H. H. (1993) *Appl. Spectrosc. 47*, 1513−1518.
49. Ma, J., Yee, A., Brewer, H. B., Jr., Das, S., and Potter, H. (1994) *Nature 372*, 92−94.
50. Brunden, K. R., Richter-Cook, N. J., Chaturvedi, N., and Frederickson, R. C. (1993) *J. Neurochem. 61*, 2147−2154.
51. Salomon, A. R., Marcinowski, K. J., Friedland, R. P., and Zagorski, M. G. (1996) *Biochemistry 35*, 13568−13578.
52. Kelly, J. W. (1996) *Curr. Opin. Struct. Biol. 6*, 11−17.

BI002005E